Plasmonically induced reflection in metal–insulator–metal waveguides with two silver baffles coupled square ring resonator*

Zhi-Dong Zhang(张志东)[1,2], Lian-Jun Ma(马连俊)[2], Fei Gao(高飞)[4], Yan-Jun Zhang(张彦军)[1,2], Jun Tang(唐军)[1,2], Hui-Liang Cao(曹慧亮)[1,2,†], Bin-Zhen Zhang(张斌珍)[1,2], Ji-Cheng Wang(王继成)[3], Shu-Bin Yan(闫树斌)[1,‡], and Chen-Yang Xue(薛晨阳)[1,2]

[1] *Science and Technology on Electronic Test & Measurement Laboratory, North University of China, Taiyuan* 030051, *China*
[2] *School of Instrument and Electronics, North University of China, Taiyuan* 030051, *Chin*
[3] *School of Science, Jiangsu Provincial Research Center of Light Industrial Optoelectronic Engineering and Technology, Jiangnan University, Wuxi* 214122, *China*
[4] *Xianyang Office, Xi'an Military Representative Bureau, PLAGF, Xianyang* 712000, *China*

(Received 20 April 2017; revised manuscript received 12 July 2017; published online 20 November 2017)

A plasmonic waveguide coupled system that is composed of a square ring cavity and a metal–insulator–metal (MIM) waveguide with two silver baffles is proposed. The transmission and reflection properties of the proposed plasmonic system are investigated numerically using the finite element method. The normalized H_z field distributions are calculated to analyze the transmission mode in the plasmonic system. The extreme destructive interference between light mode and dark mode causes plasmonically induced reflection (PIR) window in the transmission spectrum. The PIR window is fitted using the coupled mode theory. The analytical result agrees with the simulation result approximately. In addition, the PIR window can be controlled by adjusting structural parameters and filling different dielectric into the MIM waveguide and the square ring cavity. The results provide a new approach to designing plasmonic devices.

Keywords: surface plasmon polaritons, plasmonically induced reflection, metal–insulator–metal, finite element method

PACS: 42.79.Gn, 42.82.Et, 42.90.+m **DOI:** 10.1088/1674-1056/26/12/124212

1. Introduction

Surface plasmon polaritons (SPPs) are transverse electromagnetic waves that propagate along the metal–dielectric interface and decay away from the metal–dielectric interface.[1] Thus, SPPs can overcome the classical diffraction limit and enable the manipulation of light on a nano-scale.[2] Many photonic devices based on SPP have been demonstrated and realized, such as biological and chemical sensors,[3–5] filters,[6,7] and all-optical switches.[8] Recently, some novel plasmonic phenomena have been found in SPP waveguide coupled resonator systems, for example, electromagnetically induced transparency-like (EIT-like), coupled-resonator-induced transparency (CRIT),[9] and phase-coupled plasmon-induced transparency.[10,11]

As a quantum interference phenomenon, EIT occurs in atomic system due to the destructive quantum interference between two excitation pathways.[12] The EIT response window has a potential application in optical data storage. However, the harsh conditions required for EIT implementation, such as low-temperature environments and stable gas lasers, restrict its development. The plasmonic-induced transparency (PIT) effect, which is analogous to EIT, can be easily achieved in plasmonic waveguide coupled systems,[13–16] and can be used in many fields, such as molecular-scale coherent light source,[17] multiple resonators,[18] multimode stub resonator,[19] plasmonic circuits,[20] and one-terminal-closed resonator.[21] Like the EIT effect, PIT and CRIT have also slow light effect.[22,23] By contrast, plasmonically induced reflection (PIR) has important potential applications in photonic device and plasmonic sensing.[24] Li *et al.* designed an MIM waveguide coupled resonator system, which can realize the PIR effect and can also control the number of the transmission dips.[25] Asgari and Granpayeh obtained the PIR window in the midinfrared (MIR) region by the graphene-coupled side resonators, which is beneficial to the MIR optical communication[26] because the narrow line width can avoid signal jamming in the optical communication. Therefore, it is the key issue for designing optical device with narrower line width.

*Project supported by the National Natural Science Foundation of China (Grant Nos. 61605177, 61275166, and 11504139), the National Science Fund for Distinguished Young Scholars, China (Grant No. 61525107), the Natural Science Foundation of Jiangsu Province, China (Grant No. BK20140167), the Natural Science Foundation of Shanxi Province, China (Grant No. 201601D011008), the Fund Program for the Scientific Activities of Selected Returned Overseas Professionals in Shanxi Province, China, the Program for the Top Young and Middle-aged Innovative Talents of Higher Learning Institutions of Shanxi Province, China, and the North University of China Science Fund for Distinguished Young Scholars.

†Corresponding author. E-mail: caohuiliang@nuc.edu.cn
‡Corresponding author. E-mail: shubin_yan@nuc.edu.cn

© 2017 Chinese Physical Society and IOP Publishing Ltd

In this paper, therefore, a plasmonic waveguide system that consists of an MIM waveguide with two silver baffles and a square ring cavity is proposed and investigated numerically. The transmission spectra, reflection spectra, and magnetic H_z field distributions are calculated using finite element method (FEM). We achieve a distinct PIR window by changing the coupling distance, the size of square ring, and the refractive index of the filling dielectric. The coupled mode theory (CMT)[27,28] is employed to explain the physics mechanism of PIR effect.

2. Structure and analysis method

The basic scheme of the proposed plasmonic waveguide coupled resonator system is shown in Fig. 1, which is composed of a square ring cavity and MIM waveguide with two silver baffles. The white areas and green areas represent air ($\varepsilon_{\rm d}$) and silver ($\varepsilon_{\rm m}$), respectively. This two-dimensional model is symmetrical with respect to the reference line (red dash-line). The MIM waveguide is separated by two silver baffles with width $d = 20$ nm, which result in the formation of a Fabry–Perot (FP) cavity. The length of the FP cavity is $L = 500$ nm. The coupled distance is $h = 60$ nm between the square ring and the FP cavity. The width of the MIM waveguide and square ring are fixed at 50 nm. Therefore, only the fundamental transverse magnetic (TM) mode is supported in the present model. The SPPs are excited at the left end of the MIM waveguide and propagate into the MIM waveguide.

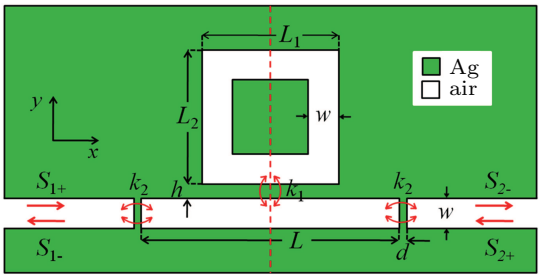


Fig. 1. (color online) Scheme of the proposed structure. The structure is composed of an MIM waveguide with two silver baffles and a square ring cavity.

The permittivity of Ag is described by the Debye–Drude model[29]

$$\varepsilon_{\rm m}(\omega) = \varepsilon_\infty + (\varepsilon_s - \varepsilon_\infty)/(1 + {\rm i}\omega\tau) + \sigma/{\rm i}\omega\varepsilon_0, \tag{1}$$

where $\varepsilon_\infty = 3.8344$ is the permittivity of infinite angular frequency; $\varepsilon_s = -9530.5$ is the static permittivity; $\tau = 7.35 \times 10^{-15}$ s is the relaxation time; $\sigma = 1.1486 \times 10^7$ S/m is the conductivity; $\varepsilon = 8.854 \times 10^{-12}$ F/m is the permittivity of vacuum. The resonance conditions of FP cavity determined by the standing wave theory are described as[30]

$$\lambda = \frac{2n_{\rm eff}L}{m - \phi/\pi}, \quad m = 1, 2, 3, \ldots, \tag{2}$$

where L is the length of the cavity, ϕ is the phase shift due to reflection, and m is an integer. The ${\rm Re}(n_{\rm eff})$ is the real part of the effective refractive index, which is obtained from ${\rm Re}(n_{\rm eff}) = \sqrt{(\varepsilon_{\rm m} + (k/k_0)^2)}$, where $k_0 = 2\pi/\lambda_0$ is the free-space wave vector. k can be solved from the dispersion function:

$$\tanh(kw) = \frac{-2k\dfrac{\varepsilon_{\rm d}}{\varepsilon_{\rm m}}\sqrt{k_0^2(\varepsilon_{\rm d} - \varepsilon_{\rm m}) + k^2}}{k^2 + \left(\dfrac{\varepsilon_{\rm d}}{\varepsilon_{\rm m}}\right)^2 (k_0^2(\varepsilon_{\rm d} - \varepsilon_{\rm m}) + k^2)}, \tag{3}$$

where w is the width of the insulator in the MIM waveguide, k is the wave vector. $\varepsilon_{\rm d}$ and $\varepsilon_{\rm m}$ are the dielectric constants of the insulator and the metal, respectively.

In order to illustrate the generation of the PIR window of this MIM waveguide coupled resonator, the CMT is introduced in this paper. The FP cavity and square ring cavity are denoted as A and B, respectively. Therefore, the time-evolution normalized amplitude A of the FP cavity and B of the square ring cavity are expressed as[31]

$$\frac{{\rm d}A}{{\rm d}t} = \left({\rm j}\omega_A - k_1^2 - k_2^2\right)A + k_2 S_{1+} + k_1 B, \tag{4}$$

$$\frac{{\rm d}B}{{\rm d}t} = \left({\rm j}\omega_B - k_1^2\right)B + k_1 A, \tag{5}$$

where k_1 is the coupling coefficient between the FP cavity and the square ring resonator k_2 is the coupling coefficient between the MIM waveguide and FP cavity, k_3 and k_4 are the decay rates of internal loss in the FP cavity and the square ring resonator, respectively and can be neglected, the amplitudes of SPPs are normalized to the incident power and denoted by S_{i+} and S_{i-} ($i = 1$ or 2), ω_A and ω_B are the resonance frequencies of the FP cavity and the square ring, respectively. Given energy conservation, the amplitudes of the input and output SPP waves can be described as:

$$S_{1-} = S_{1+} + k_2 A, \tag{6}$$

$$S_{2-} = S_{2+} + k_2 A. \tag{7}$$

The SPPs are launched into the system only from the input port of the MIM waveguide, i.e. $S_{2+} = 0$. The transmittance can be expressed as

$$T = \left|\frac{S_{2-}}{S_{1+}}\right|^2 = \left|\frac{k_2^2\left[{\rm j}(\omega - \omega_{\rm B}) + k_1^2\right]}{\left[{\rm j}(\omega - \omega_A) + k_1^2 + k_2^2\right]\left[{\rm j}(\omega - \omega_{\rm B}) + k_1^2\right] - k_1^2}\right|^2. \tag{8}$$

The SPPs of the FP cavity are excited directly by the incident light, and they are in the bright mode, whereas the SPPs of the square ring resonator are excited by the coupled FP cavity, and they are regarded as dark mode.

3. Results and discussion

To better understand the transmission and reflection properties of the proposed structure, the transmission spectrum and reflection spectrum of the MIM waveguide with two silver baffles are calculated and shown in Fig. 2(a). Each dip of the reflection spectrum is corresponding to a peak of the transmission spectrum. The corresponding structures are shown in the two insets and the structural parameters are $L = 500$ nm, $L_1 = 194$ nm, $L_2 = 194$ nm, $d = 20$ nm, and $h = 60$ nm. For the MIM waveguide with two silver baffles, three transmission peaks and reflection dip are observed in the transmission spectrum and the reflection spectrum. These peaks exhibit distinct band-pass characteristics. The normalized H_z field distributions at different resonance wavelengths ($\lambda = 0.424$ μm, $\lambda = 0.526$ μm, and $\lambda = 0.757$ μm) are shown in Fig. 2(b). For $\lambda = 0.526$ μm and $\lambda = 0.424$ μm, 2 and 1.5-order standing-wave resonance modes are formed, respectively. For $\lambda = 0.757$ μm, 1order standing-wave resonance mode is formed in the FP cavity. For the MIM waveguide side-coupled square ring cavity, figure 2(c) shows the transmission spectrum and reflection spectrum of the MIM waveguide side-coupled square ring cavity. The normalized H_z field distributions of the MIM waveguide side-coupled square ring cavity are displayed in Fig. 2(d). The one- and two-order mode distributions are formed at $\lambda = 0.757$ μm and $\lambda = 0.473$ μm, respectively. In addition, we find that the resonance peak is red-shifted linearly with increasing L_1, which is in accordance with Eq. (2). The MIM waveguide with two silver baffles owns a band pass characteristics, but the MIM waveguide side-coupled square ring cavity has a band stop characteristics at $\lambda = 0.757$ μm. Therefore, we combine the FP cavity and square ring cavity to generate PIR window when $L_1 = 194$ nm.

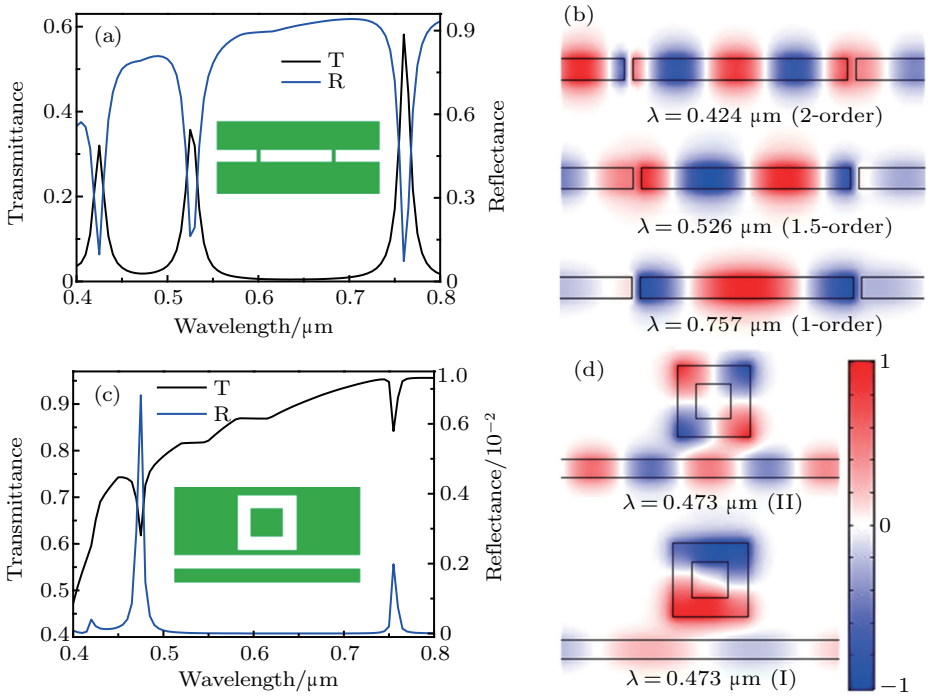


Fig. 2. (color online) (a) Transmission spectrum and reflection spectrum of the MIM waveguide with only two silver baffles. (b) Normalized Hz field distributions that correspond to the transmission peaks of the MIM waveguide with two silver baffles. (c) Transmission spectrum and reflection spectrum of the MIM waveguide side-coupled square ring cavity. (d) Normalized Hz field distributions of the transmission dip of the MIM waveguide side-coupled square ring cavity.

Figure 3(a) presents the transmission spectra in 0.720.8 μm of the MIM waveguide with two silver baffles and of the MIM waveguide with two-silver-baffle side-coupled square ring cavity system. Compared with the transmission spectrum of the MIM waveguide with two silver baffles, two transmission peaks and one dip are observed in that of the MIM waveguide with two silver-baffle side-coupled square ring cavity system. The blue solid curve is obtained by solving Eq. (8) with $k_1 = 0.033$ and $k_2 = 0.24$, which are approximately agree with the simulated results. Figure 3(b) shows the transmission spectrum and corresponding reflection spectrum of the MIM waveguide with two-silver-baffle side-coupled square ring cavity system. The dip and peaks of the transmission spectrum are corresponding to the peak and dips of the reflection spectrum, respectively. So the dip of the transmission spectrum can be regarded as PIR window. To explain the origin of PIR, the normalized H_z field distributions at different resonance wavelengths are calculated. The normalized H_z field distributions of the MIM waveguide with $\lambda = 0.757$ μm (marked as A) are shown in Fig. 3(c). For the MIM waveguide with two-silver-baffle side-coupled square ring cavity, the normalized H_z field distributions at $\lambda = 0.752$ μm (marked as

B) show that there is in-phase between the square ring cavity and FP cavity. At $\lambda = 0.757$ μm, the SPPs are mainly restricted in the square ring cavity. Hardly any SPPs propagate into the right waveguide from the FP cavity (marked as C). At $\lambda = 0.765$ μm (marked as D), the strong normalized H_z field mainly appears in the FP cavity and weak normalized H_z field occurs in the square ring cavity. The normalized H_z field distributions show that there is anti-phase between the square ring cavity and FP cavity. The mode (bright mode) of the FP cavity is excited directly by incident light, but the square ring cavity mode (dark mode) is excited indirectly by the mode of the FP cavity. Therefore, PIR window is caused by the extreme destructive interference between the bright mode and dark mode.

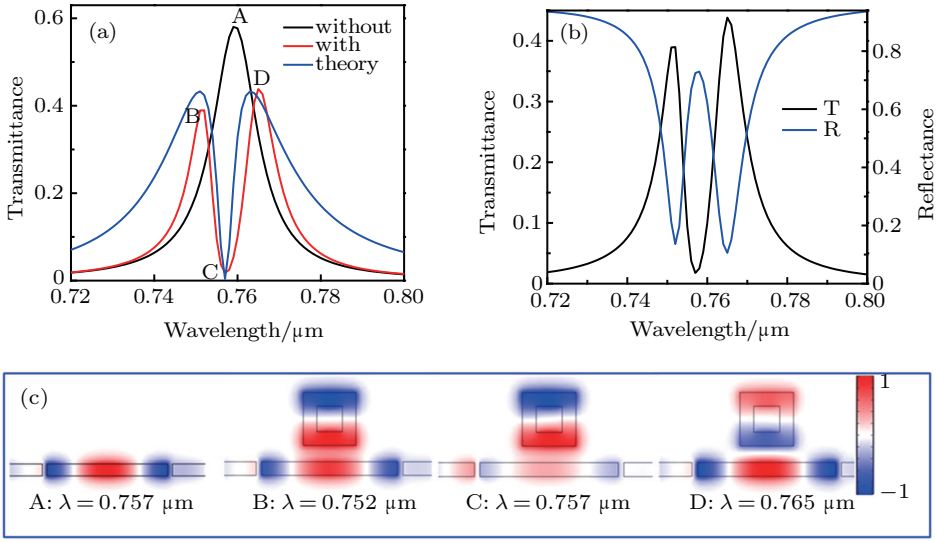


Fig. 3. (color online) (a) Transmission spectra of the coupled waveguide system with and without square ring cavity and theoretical analysis. (b) Transmission spectrum and reflection spectrum of the coupled waveguide system with square ring cavity. (c) The magnetic H_z field distributions of transmission peaks and dip marked as A, B, C, and D.

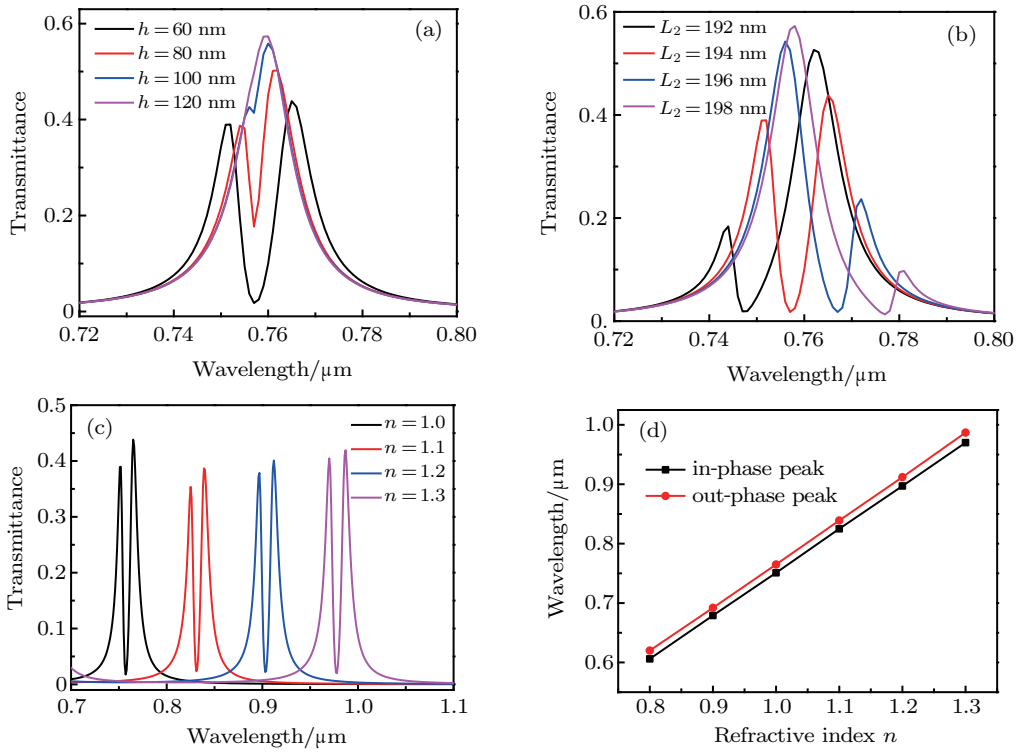


Fig. 4. (color online) (a) Transmission spectra of different values of coupling distance h, (b) different values of L_2 of the square ring cavity and (c) different values of refractive index n. (d) Relationship between resonance peak wavelength λ and refractive index n.

The influences of the geometrical parameters on the transmission spectra are investigated. Figure 4(a) shows the transmission spectra as h increases from 60 nm to 120 nm in steps of 20 nm with $L_1 = L_2 = 194$ nm and $n = 1.0$. The transmittance increases and the PIR window gradually disappears as h increases. When $h = 120$ nm, the profile of the transmission

spectrum is similar to that of the MIM waveguide with two silver baffles. Figure 4(b) shows that the transmission spectra for L_2 increasing from 192 nm to 198 nm when h is fixed at 60 nm. The transmittance of the in-phase mode peak increases but the transmittance of the anti-phase mode peak decreases as L_2 increases. To investigate the sensitivity of PIR window to the refractive index, the transmission spectrum of the air is calculated after replacing the different dielectrics with $h = 60$ nm and $L_2 = 194$ nm. The transmission spectra of dielectric refractive index $n = 1.0$, 1.1, 1.2, 1.3 are displayed in Fig. 4(c). As n increases, the in-phase mode peak and the anti-phase mode peak are red-shifted. In addition, the effective refractive index n_{eff} increases as n increases. Therefore, the SPP resonance peaks are red-shifted with increasing L_2 and n according to Eq. (2), which agrees approximately with the simulation result (as shown in Figs. 4(b) and 4(c)). In addition, the sensitivity of the proposed structure is $S = \delta\lambda/\delta n = 700$ nm/RIU and FOM $=$ S/FWHM $= 87.5$ and 100 correspond to left and right peaks in Fig. 4(c), respectively. Its FOM is larger than the previous result (FOM $= 63$).[32] Figure 4(d) shows the wavelength of the resonance peak as a function of the refractive index. The in-phase mode peak and the out-of-phase mode peak change linearly with the refractive index n, and their slopes are equal.

4. Conclusions and perspectives

In this work a plasmonic waveguide coupled resonator system that consists of a square ring cavity and MIM waveguide with two silver baffles is proposed and investigated using FEM in this paper. The extreme destructive interference between the bright mode in the FP cavity and dark mode in the square ring cavity leads to the generation of the PIR window. The line width of PIR window is narrower than that of previous structure in our proposed plasmonic system. The normalized H_z field distributions are employed to analyze the transmission mode in the plasmonic system. Moreover, CMT is employed to explain the result, which agrees with the simulations approximately. In addition, the PIR window can be flexibly controlled by adjusting structural parameters and changing dielectric. The proposed structure has potential applications in optical communication devices.

References

[1] Barnes W L, Dereux A and Ebbesen T W 2003 *Nature* **424** 824
[2] Ozbay E 2006 *Science* **311** 189
[3] Chen Z, Song X, Jiao R, Duan G, Wang L and Yu L 2015 *IEEE Photon. J.* **7** 4801408
[4] Chen J J, Li Z, Zou Y J, Deng Z L, Xiao J H and Gong Q H 2013 *Plasmon.* **8** 1627
[5] Ho H P, Yuan W, Wong C L and Lin C 2007 *Opt. Commun.* **275** 491
[6] Ma J Y, Xu C, Liu S J, Zhang D W, Jin Y X, Fan Z X and Shao J D 2009 *Chin. Phys. B* **18** 1029
[7] Lin X S and Huang X G 2008 *Opt. Lett.* **33** 2874
[8] Bian Z Y, Liang R S, Zhang Y J, Yi L X, Lai G and Zhao R T 2015 *Chin. Phys. B* **24** 107801
[9] Smith D D, Lepeshkin N N and Schweinsberg Al 2006 *Opt. Commun.* **264** 163
[10] Kekatpure R D, Barnard E S, Cai W and Brongersma M L 2010 *Phys. Rev. Lett.* **104** 243902
[11] Li B X, Li H J and Zeng L L 2015 *IEEE. Photon. J.* **7** 1
[12] Fleischhauer M, Imamoglu A and Marangos J P 2005 *Rev. Mod. Phys.* **77** 633
[13] Jin X R, Lu Y, Zheng H, Lee Y, Rhee J Y, Kim K W and Jang W H 2011 *Opt. Commun.* **284** 4766
[14] Zhu Y, Hu X Y, Yang H and Gong Q H 2014 *Sci. Rep.* **4** 3752
[15] Deng Z L, Dong J W, Wang H Z, Cheng S H and Li J S 2013 *AIP Advances* **3** 032138
[16] Piao X J, Yu S K, Koo S, Lee K and Park N 2011 *Opt. Express* **19** 10907
[17] Han Z H and Bozhevolnyi S I 2011 *Opt. Express* **19** 3251
[18] Wen K H, Hu Y H, Chen L, Zhou J Y, He M, Lei L and Meng Z M 2015 *IEEE. Photon. J.* **7** 1
[19] Yun B F, Hu G H and Cui Y P 2013 *Opt. Commun.* **305** 17
[20] Deng Z L and Dong J W 2013 *Opt. Express* **17** 20291
[21] Shang X J, Li X F, Wang L L, Zhai X, Lin Q, Wang B X, Liu G D, Xia S X and Li Q 2015 *Eur. Phys. J. B* **88** 144
[22] Wang N, Zhang Y D and Yuan P 2011 *Chin. Phys. B* **20** 04420
[23] Nan W, Zhang Y D, Wang J F, Tian H, Wang H, Zhang X N, Zhang J and Yuang P 2009 *Acta Phys. Sin.* **58** 7672 (in Chinese)
[24] Vafapour Z and Zakery A 2016 *Plasmonics* **11** 609
[25] Li H J, Zhai X and Wang L L 2015 *Appl. Phys. Express* **8** 092201
[26] Asgari S and Granpayeh N 2017 *J. Nanophoton.* **11** 026012
[27] Haus H A and Huang W 1991 *Proc. IEEE* **79** 1505
[28] Li Q, Wang T, Su Y, Yan M and Qiu M 2010 *Opt. Express* **18** 8367
[29] Gai H, Wang J and Tian Q 2007 *Appl. Opt.* **46** 2229
[30] Xu Q, Sandhu S, Povinelli M L, Shakya J, Fan S H and Lipson M 2006 *Phys. Rev. Lett.* **96** 123901
[31] Lai G, Liang R S, Zhang Y J, Bian Z Y, Yi L X, Zhan G Z and Zhao R T 2015 *Opt. Express* **23** 6554
[32] TangY, Zhang Z D, Wang R B, Hai Z Y, Xue C Y, Zhang W D and Yan S B 2017 *Sensors* **17** 784